Quinolinic acid/tryptophan ratios predict neurological disease in SIV-infected macaques and remain elevated in the brain under cART

Julia L. Drewes,

Department of Molecular and Comparative Pathobiology, Johns Hopkins University School of Medicine, Baltimore, MD 21205, USA

Kelly A. Meulendyke,

Department of Molecular and Comparative Pathobiology, Johns Hopkins University School of Medicine, Baltimore, MD 21205, USA

Zhaohao Liao,

Department of Molecular and Comparative Pathobiology, Johns Hopkins University School of Medicine, Baltimore, MD 21205, USA

Kenneth W. Witwer,

Department of Molecular and Comparative Pathobiology, Johns Hopkins University School of Medicine, Baltimore, MD 21205, USA

Lucio Gama,

Department of Molecular and Comparative Pathobiology, Johns Hopkins University School of Medicine, Baltimore, MD 21205, USA

Ceereena Ubaida-Mohien,

Department of Molecular and Comparative Pathobiology, Johns Hopkins University School of Medicine, Baltimore, MD 21205, USA

Ming Li,

Department of Molecular and Comparative Pathobiology, Johns Hopkins University School of Medicine, Baltimore, MD 21205, USA

Francesca M. Notarangelo,

Maryland Psychiatric Research Center, Department of Psychiatry, University of Maryland School of Medicine, Baltimore, MD 21228, USA

Patrick M. Tarwater,

Division of Biostatistics and Epidemiology, Texas Tech University Health Science, Center, El Paso, TX 79902, USA

Robert Schwarcz,

Corresponding author: M. Christine Zink. mczink@jhmi.edu. Phone: (410) 955-9770. Fax: (410) 955-9823.

Conflict of Interest

The authors declare that they have no conflicts of interest.

Maryland Psychiatric Research Center, Department of Psychiatry, University of Maryland School of Medicine, Baltimore, MD 21228, USA

David R. Graham, and
Department of Molecular and Comparative Pathobiology, Johns Hopkins University School of Medicine, Baltimore, MD 21205, USA

M. Christine Zink
Department of Molecular and Comparative Pathobiology, Johns Hopkins University School of Medicine, Baltimore, MD 21205, USA

Abstract

Activation of the kynurenine pathway (KP) of tryptophan catabolism likely contributes to HIV-associated neurological disorders. However, KP activation in brain tissue during HIV infection has been understudied, and the effect of combination anti-retroviral therapy (cART) on KP induction in the brain is unknown. To examine these questions, tryptophan, kynurenine, 3-hydroxykynurenine, quinolinic acid, and serotonin levels were measured longitudinally during SIV infection in striatum and CSF from untreated and cART-treated pigtailed macaques. mRNA levels of KP enzymes also were measured in striatum. In untreated macaques, elevations in KP metabolites coincided with transcriptional induction of upstream enzymes in the KP. Striatal KP induction was also temporally associated - but did not directly correlate - with serotonin losses in the brain. CSF quinolinic acid/tryptophan ratios were found to be the earliest predictor of neurological disease in untreated SIV-infected macaques, outperforming other KP metabolites as well as the putative biomarkers Interleukin-6 (IL-6) and Monocyte chemoattractant protein-1 (MCP-1). Finally, cART did not restore KP metabolites to control levels in striatum despite control of virus, though CSF metabolite levels were normalized in most animals. Overall these results demonstrate that cerebral KP activation is only partially resolved with cART, and that CSF QUIN/TRP ratios are an early, predictive biomarker of CNS disease.

Keywords

HIV; SIV; kynurenine; quinolinic acid; tryptophan; serotonin

Introduction

Though combination anti-retroviral therapy (cART) has been successful in lessening the severity of neurological complications in HIV-infected individuals, the prevalence of neurological impairments and psychiatric ailments such as depression continues to increase, prompting a call for biomarkers of these disorders and a better understanding of their underlying pathogenesis (Robertson et al. 2007; Heaton et al. 2010). These neurological disorders afflict a substantial proportion of HIV-infected individuals, with estimates ranging from 20–60% despite access to cART (Robertson et al. 2007; Heaton et al. 2010; Chibanda et al. 2014; Ances and Ellis 2007). Furthermore, cognitive impairment and depression are risk factors for each other, decrease cART compliance, and are associated with a faster progression to AIDS and mortality (Chibanda et al. 2014; Del Guerra et al. 2013). Enhanced catabolism of tryptophan (TRP) through the kynurenine pathway (KP) may contribute to the

etiology of both of these disorders by generating neurotoxic levels of KP metabolites and diverting TRP away from serotonin synthesis, though evidence in brain tissue has remained limited.

Indoleamine 2,3-dioxygenase (IDO) controls the first and rate-limiting step of the KP: the cleavage of TRP into L-formylkynurenine. A series of biologically active metabolites are then generated, including the pivotal metabolite kynurenine (KYN) and the neurotoxic metabolites 3-hydroxykynurenine (3HK) and quinolinic acid (QUIN), which are elevated in the CSF and/or brain during HIV/SIV infection (Sardar et al. 1995; Heyes et al. 1991; Heyes et al. 1989; Heyes et al. 1992b). The shunting of TRP down the KP may also deplete TRP reservoirs in the brain and thereby negatively impact the synthesis of the neurotransmitter serotonin, a deficiency of which is a risk factor for the development of depression (Ruhe et al. 2007; Smith et al. 1997). Accordingly, TRP and serotonin levels are reduced in the CSF of HIV-infected individuals, particularly those in later stages of disease (Larsson et al. 1989; Kumar et al. 2001; Fuchs et al. 1990).

Together with a reduction in serotonin formation, increased catabolism along the QUIN axis of the KP may therefore play a causative role in several HIV-associated neurological disorders. However, while residual elevations in peripheral KP metabolites have been demonstrated in several cohorts despite successful suppression of viremia with cART (Gendelman et al. 1998; Jenabian et al. 2013; Chen et al. 2014), no study as of yet has examined KP activation in the brain following cART, nor has the timing of KP activation been established in the CNS. We reasoned that a longitudinal assessment of these phenomena in brain and CSF samples from our well-established, accelerated simian model of HIV-associated neurological disease would provide new insights into the relationship between TRP metabolism and disease trajectory and might reveal useful biomarkers for both diagnosis and intervention (Zink et al. 2010; Clements et al. 2008). Using this model, we demonstrate the biphasic elevation of KP metabolites and upstream KP enzymes in the brain, concomitant losses in striatal serotonin, and residual activation of the KP under cART. We also propose the use of CSF QUIN/TRP ratios as a sensitive, early predictive biomarker of neurological disease. Overall these data shed light on early events leading to neurological disease and provide important therapeutic targets and biomarkers applicable to patient cohorts.

Materials and Methods

Animals

Archived samples from 84 pigtailed macaques (*Macaca nemestrina*) were studied, of which 10 were uninfected controls and 74 were inoculated intravenously with SIV/DeltaB670 and SIV/17E-Fr as previously described (Zink et al. 1999). Beginning at day 12 p.i., 5 of the infected macaques received combination antiretroviral therapy (cART) which suppressed plasma viremia to <100 SIV RNA copy eq./mL by day 70 p.i. (Dinoso et al. 2009). The 4-drug cART regimen consisted of 270 mg/kg of the protease inhibitor atazanavir (Bristol-Myers Squibb), 10 mg/kg of the integrase inhibitor L-870812 (Merck), and 205 mg/kg of the protease inhibitor saquinavir (Roche) administered orally twice/day; as well as 30 mg/kg of the nucleotide reverse transcriptase inhibitor PMPA (Gilead) administered subcutaneously

once daily. The 5 cART-treated animals were euthanized 161–175 days p.i. after approximately 100 days of plasma viremia suppression. Infected, untreated macaques were euthanized during various stages of disease (4, 7, 10, 14, 21, 35, 42, 56, and 84 days p.i.). Some animals were euthanized prior to their planned euthanasia date due to presentation of clinical symptoms that met euthanasia criteria (Weed et al. 2003), and are therefore grouped with SIV terminal animals (T or SIVT) in the figures. All animals had longitudinal CSF draws performed at the following time points: at least 3 pre-infection draws, then on days 7, 10, 14, 21, 28, and every two weeks thereafter. CSF was centrifuged at 1300 g for 15 min to remove any cells before being frozen at −80°C. All animals were euthanized in accordance with federal guidelines and institutional policies. Macaques were euthanized under veterinary supervision with intravenous sodium pentobarbital while under deep ketamine sedation; macaques were perfused with sterile PBS and tissues were collected and either frozen until use or fixed. All animal studies were approved by the Johns Hopkins Animal Care and Use Committee; all animals were humanely treated in accordance with federal guidelines and institutional policies.

Immunohistochemisry, Histopathology, and Encephalitis Scoring

Immunohistochemical staining for MHC II and CD68 in subcortical white matter adjacent to striatum and APP in corpus callosum was quantitated in a blinded fashion as previously described (Zink et al. 2010; Mankowski et al. 2002). For encephalitis scoring, five regions of brain (basal ganglia, thalamus, parietal cortex, cerebellum, midbrain) were stained with hematoxylin and eosin, blinded, and examined by two pathologists, who scored the brain regions on a scale from 0–3 based on the presence of perivascular macrophage-rich cuffs, multi-nucleated giant cells and gliosis. The scores from all five brain regions were averaged to obtain the encephalitis score for each animal.

Brain Tissue Homogenization

Three millimeter punches were taken from perfused striatum of snap-frozen pigtailed macaque brain tissue. Samples were weighed and diluted 1/20 (weight/volume) with ice-cold 0.1% ascorbic acid and sonicated 3 times at 30% amplitude for 3 sec on ice.

Metabolite Extraction from Brain Homogenates

On ice, brain homogenates (50 μL) were spiked with 50 μL of a heavy standard solution containing 1 μM [^{2}H$_5$] tryptophan (CDN Isotopes, Quebec, Canada), 5 μM [^{2}H$_6$] kynurenine (custom synthesis from Sigma Aldrich Isotec), and 0.2 μM [^{2}H$_3$] quinolinic acid (custom synthesis from Synfine, Ontario, Canada). Samples were spiked with 50 μL of −20°C acetone and centrifuged at 20,000 g for 5 min. The supernatants (120 μL) were transferred to microcentrifuge tubes, spiked with 50 μL of a 2:5 ratio methanol:chloroform, and centrifuged at 20,000 g for 10 min. The aqueous layers (80 μL) were transferred to glass vials and evaporated to dryness. Samples were derivatized with 120 μL of 2,2,3,3,3-pentafluoro-1-propanol (Sigma) and 135 μL of pentafluoropropionic anhydride (Sigma) by heating at 75°C for 30 min. Derivatized samples were evaporated to dryness and stored at −80°C.

Metabolite Extraction from CSF

CSF samples (25 μL) were mixed with 25 μL of ice-cold 0.2% ascorbic acid and 50 μL of the heavy standard mixture. Fifty microliters of −20°C acetone was added and samples were centrifuged at 20,000 g for 10 min. CSF supernatants (120 μL) were transferred to glass vials, dried, and then derivatized as above.

GC/MS/MS Analysis of Metabolites

GC/MS/MS conditions and multiple reaction monitoring (MRM) transitions were as previously described (Notarangelo et al. 2012). De-identified samples were injected in a randomized order at least twice. Data were analyzed with Agilent MassHunter software, Build B.04. Peak areas for each compound were normalized to their heavy standards, then fit to their matrix-spiked light standard curve based on the standard addition method. No heavy standard was spiked in for 3HK, which was instead normalized to heavy KYN because of their similar properties.

Serotonin, IL-6, and MCP-1 ELISAs

Striatal serotonin levels and CSF IL-6 and MCP-1 were measured in duplicate by ELISA (serotonin: Eagle Biosciences; IL-6 and MCP-1: R&D Systems). Samples were read on a microplate reader (BioRad) at the recommended wavelength.

Nanostring nCounter gene expression analysis

RNA samples from striatum were run in a randomized order on a custom Nanostring nCounter codeset as previously described (Meulendyke et al. 2014). Only the 7 genes involved in TRP metabolism were included in the present analysis. Positive control corrected data were normalized to the geometric mean of three housekeeping genes (ACTB, GAPDH, and TBP). Trends in IDO1 mRNA expression in brain were independently verified by qRT-PCR.

qRT-PCR

SIV RNA was analyzed by qRT-PCR as previously described (Witwer et al. 2009).

Statistical Analysis

For striatal metabolite data, the Mann-Whitney U test was performed to compare peak values during acute infection (determined by the time point with the highest median between days 0 – 14 p.i. for each metabolite, or nadir for tryptophan and serotonin), all values during asymptomatic infection (day 21 p.i.), and all values during chronic infection (between day 35 p.i. and terminal) against uninfected controls. P-values for these comparisons were Bonferroni adjusted due to multiple comparisons. In a second analysis, the Mann-Whitney U test was performed to compare moderate/severe encephalitis animals to none/mild encephalitis animals during chronic infection.

For CSF metabolite data, analyses were performed on the fold change data. A Wilcoxon signed rank test comparing values to a theoretical value of "1" was used to examine whether the peak (nadir for tryptophan and serotonin) for each animal during acute infection, or

median values for each animal during asymptomatic and chronic infection, were significantly different from their respective pre-infection values. *P*-values for these comparisons were Bonferroni adjusted due to multiple comparisons. In a second analysis the Mann-Whitney U test was performed comparing the two encephalitis outcomes at each time point beginning at day 21 p.i. The earliest day with significant difference was indicated with a downward arrow on the graphs. One severe animal displayed hemolysis in the day 21 and day 42 p.i. CSF samples. The last value carried forward imputation for longitudinal data was used to replace these values; i.e., the value from day 14 p.i. was used for the day 21 p.i. time point, and the value from day 28 p.i. was used for the day 42 p.i. time point.

For striatal Nanostring nCounter mRNA expression data, the 5 KP genes that were above background thresholds were subjected to a Kruskal-Wallis rank test followed by Benjamini Hochberg false discovery rate (FDR) corrections based on the simultaneous measurement of these 5 genes. For any genes for which a significant Benjamini-Hochberg corrected *P*-value was obtained ($P < 0.05$), Mann-Whitney U tests were then performed in the same manner as described for striatal metabolites.

For correlation studies a Spearman's rank correlation was used.

For cART metabolite data in striatum a Mann-Whitney U test was performed to compare Uninf vs. cART; the SIVT group was shown for reference purposes only.

Microsoft Office 2011 Excel was used to prepare all tables and to perform multiple comparison corrections (both Benjamini Hochberg and Bonferroni corrections). GraphPad Prism 6.0 was used to prepare all other figures and statistical analyses.

Results

KP metabolites are elevated biphasically in the striatum during SIV infection

To determine the overall effect of infection on KP induction in the brain, we first examined the levels of TRP and KP metabolites in striatal samples from SIV-infected macaques euthanized at various points throughout infection. The list of striatal samples and their associated neuropathological features are shown in Table 1. The striatal region was chosen because it demonstrates pronounced neuropathological changes during HIV/SIV infection (McArthur et al. 2005) and is highly susceptible to both QUIN-mediated excitotoxicity (Schwarcz et al. 1983) and 3HK-mediated oxidative stress (Okuda et al. 1998). Induction of KP metabolites in the brain during acute infection was determined by comparing values from the time point with the highest median (day 7 or 10 p.i.) to uninfected controls, while for TRP the time point with the lowest median was chosen (day 10 p.i.). For chronic infection, values from all of the animals euthanized during that phase (day 35 p.i.) were grouped and then compared to uninfected controls. Baseline values for the metabolites in both CSF and striatum and changes during infection are summarized in Table S1.

TRP levels in striatum were not significantly different from controls during any phase of infection ($P = 0.165$ at day 10 p.i.; $P > 0.999$ for asymptomatic and chronic infection; Fig. 1a). In contrast, levels of KP metabolites displayed robust changes in striatum. KYN levels

in infected animals were significantly higher than uninfected controls at their peak during acute infection ($P < 0.001$ at day 7 p.i.; Fig. 1b) and during the chronic phase of infection ($P < 0.001$; Fig. 1b). Levels of 3HK, the downstream metabolite of KYN, were significantly elevated during both acute ($P = 0.012$ at day 10 p.i.; Fig. 1c) and chronic infection ($P = 0.002$; Fig. 1c). QUIN was significantly elevated in the striatum during acute ($P = 0.006$ at day 7 p.i.; Fig. 1d), asymptomatic ($P = 0.048$; Fig. 1d), and chronic infection ($P < 0.001$; Fig. 1d) in the striatum of infected animals.

We also examined the KYN/TRP ratio, a widely used surrogate measure for the initial enzymatic step in the KP. Striatal KYN/TRP ratios were elevated above uninfected controls during acute ($P < 0.001$ at day 7 p.i.; Fig. 1e), asymptomatic ($P = 0.033$; Fig. 1e), and chronic infection ($P < 0.001$; Fig. 1e).

Finally, we calculated a QUIN/TRP ratio as a measure of activation through the QUIN branch of the KP. Striatal QUIN/TRP ratios were significantly elevated during acute infection ($P = 0.006$ at day 7 p.i.; Fig. 1f) and chronic infection ($P < 0.001$; Fig. 1f). These data demonstrate the biphasic nature of KP induction in the brain.

We next examined whether the animals with more severe encephalitis, as determined by histopathology, had more pronounced changes in KP metabolites as compared to animals with less severe neurological changes. Animals with moderate/severe encephalitis displayed significantly lower levels of TRP during chronic infection as compared to those with less severe encephalitis ($P = 0.045$; Fig. 1a). In accordance with their lower levels of TRP, animals with moderate/severe encephalitis had significantly higher levels of KYN, 3HK, and QUIN, as well as higher KYN/TRP and QUIN/TRP ratios, as compared to animals with none/mild encephalitis (all $P < 0.0001$ except for 3HK, which was $P = 0.0006$; Fig. 1b–f). Overall these data suggested that animals with more severe neurological lesions had more pronounced KP activation.

CSF mimics some, but not all, changes in brain KP activation

We next examined whether levels of KP metabolites in the CSF reflected changes in the brain. In contrast to brain tissue, in which minimal changes in TRP were detected, longitudinal analysis of the CSF revealed a significant early decrease in TRP levels during acute infection ($P = 0.024$ for each animal's nadir during acute infection compared to pre-infection values; Fig. 2a). TRP remained low during asymptomatic infection but was recovered in some animals by the chronic phase of infection ($P = 0.048$ and $P = 0.165$ for asymptomatic and chronic infection, respectively; Fig. 2a).

Levels of KYN and 3HK in the CSF were significantly higher at their peaks during acute infection compared to pre-infection values ($P = 0.048$; Fig. 2b; and $P = 0.024$; Fig. 2c, respectively), coincident or even preceding the acute peak in CSF viral loads (Fig. S1a). However, neither metabolite was significantly elevated later in infection, largely due to a lack of change in the animals that developed less severe neurological disease. In contrast, QUIN levels in the CSF were elevated throughout infection in all animals ($P = 0.024$ for acute, asymptomatic, and chronic infection; Fig. 2d).

KYN/TRP ratios were significantly elevated only during the peak at acute infection ($P = 0.024$; Fig. 2e), mimicking KYN alone. In contrast, persistent elevations were seen throughout acute, asymptomatic, and chronic infection for QUIN/TRP ratios ($P = 0.024$ for all phases of infection; Fig. 2f).

CSF QUIN/TRP ratios are an early predictor of encephalitis

QUIN has previously been proposed as a CSF biomarker of HIV-associated motor/cognitive disorders (Heyes et al. 1991; Martin et al. 1993; Heyes et al. 1992a), but its ability to predict neurological disease before the onset of clinical symptoms is unknown. We therefore examined whether TRP and its metabolites could differentiate between the two major encephalitis outcomes (none/mild versus moderate/severe) beginning with the asymptomatic phase of infection (day 21 p.i. onwards).

Interestingly, CSF TRP fold change values differed significantly between the two encephalitis outcomes as early as day 21 p.i. ($P = 0.036$ none/mild versus moderate/severe fold changes at day 21 p.i.; Fig. 2a), though the substantial variability in raw TRP levels limited its prognostic value in the absence of matched, pre-infection values (Fig. S1b). In contrast, CSF fold changes in KYN, 3HK, and QUIN levels did not reach significance between the two groups of encephalitis outcomes until chronic infection (all $P = 0.036$ none/ mild versus moderate/severe fold changes at day 42 p.i.; Fig. 2b–d).

The most robust predictive markers were the KYN/TRP and QUIN/TRP ratios, whose fold changes differentiated between the two encephalitis outcomes by day 28 p.i. (both $P = 0.036$ at day 28 p.i.; Fig. 2e, f). Unlike TRP levels, the striking divergence of KYN/TRP and QUIN/TRP ratios was retained in the raw data (Fig. S1f, g), which would be of importance in patient samples for which pre-infection values are often not available. Of the two ratios, however, only QUIN/TRP displayed any elevation chronically in the CSF of animals that went on to develop milder forms of encephalitis as compared to pre-infection values, suggesting that the QUIN/TRP ratio may be more sensitive than KYN/TRP at detecting small neuropathological changes. QUIN/TRP ratios also demonstrated earlier predictive power than interleukin-6 (IL-6) and monocyte chemoattractant protein-1 (MCP-1), two previously identified biomarkers of neurological disease in our model (Mankowski et al. 2004), which did not significantly differentiate the two encephalitis outcomes until day 42 p.i. in the present set of animals (Fig. S2a, b).

mRNA expression of upstream KP enzymes increases during SIV infection

We hypothesized that the changes observed in CNS KP metabolites were at least partially due to transcriptional induction of KP enzymes. To test this, mRNA from striatal tissue was analyzed for the expression levels of seven KP genes: *IDO1*, *indoleamine 2,3-dioxygenase 2* (*IDO2*), *tryptophan 2,3-dioxygenase* (*TDO2*), *kynurenine 3-monooxygenase* (*KMO*), *kynureninase* (*KYNU*), *3-hydroxyanthranilate 3,4-dioxygenase* (*HAAO*), and *quinolinate phosphoribosyltransferase* (*QPRT*).

IDO1 mRNA expression was significantly upregulated at both the peak during acute infection ($P < 0.001$ at day 4 p.i.; Fig. 3a) and during chronic infection ($P < 0.001$; Fig. 3a)

in striatum. The majority of expression values for the two other TRP dioxygenases, *IDO2* and *TDO2*, were below the threshold for quantitation at all time points in striatum and were therefore excluded.

Expression of *KMO*, which converts KYN to 3HK, approached significance during chronic infection ($P = 0.077$; Fig. 3b), while expression of *KYNU*, which converts KYN to anthranilic acid and 3HK to 3-hydroxyanthranilic acid (3HANA), was significantly upregulated chronically ($P = 0.003$; Fig. 3c). In contrast, expression of *HAAO* and *QPRT*, the downstream KP enzymes that catalyze the conversion of 3HANA to QUIN and the breakdown of QUIN into NAD+, respectively, were not significantly changed during infection.

Additionally, animals that had moderate/severe encephalitis had significantly higher expression *of IDO1, KMO*, and *KYNU mRNA* during chronic infection than animals with none/mild encephalitis (all $P < 0.0001$; Fig. 3a–c), while the expression of *HAAO* and *QPRT* did not segregate by severity of encephalitis (Fig. 3d, e). Overall, these data indicate that the upstream KP genes are preferentially regulated at the transcriptional level during infection.

Striatal QUIN/TRP ratios correlate with markers of neuropathogenesis in chronically infected animals

Given the strong associations between encephalitis severity and KP activation in the striatum, we next assessed whether QUIN/TRP ratios correlated with other, more quantitative measures of inflammation in chronically infected animals (day 35 p.i.).

Because only macrophages and microglia are thought to express the full cohort of enzymes required for conversion of TRP to QUIN in the brain (Guillemin et al. 2001), we first examined whether increases in QUIN/TRP ratios correlated with markers of macrophage/microglial activation. QUIN/TRP ratios in striatum significantly correlated with both MHC Class II ($r = 0.594$; $P = 0.006$; Fig. 4a) and CD68 protein expression ($r = 0.759$; $P < 0.0001$; Fig. 4b) in subcortical white matter adjacent to the striatum.

Striatal QUIN/TRP ratios also correlated significantly with SIV *gag* RNA in striatum ($r = 0.896$; $P < 0.0001$; Fig. 4c). The relationship between QUIN/TRP ratios and viral load was biphasic: animals with viral loads less than 10^5 copy equivalents had minimal changes in QUIN/TRP ratios, while animals with viral loads above 10^5 displayed more drastic changes in QUIN/TRP values.

Finally, although behavioral testing was not performed on the present set of animals, previous studies in our laboratory have demonstrated that elevations in amyloid precursor protein (APP) as well as CD68 protein strongly correlate with impaired performance on the bimanual motor task (Weed et al. 2003), a measure of fine motor control that parallels an important manifestation of HIV-associated motor/cognitive disorders. Though QUIN's excitotoxic effects are primarily axon-sparing and are therefore unlikely to be directly implicated in APP accumulation (Schwarcz et al. 1983), we sought to test the utility of the QUIN/TRP ratio as a surrogate measure for the multitude of inflammatory events leading to changes in neuronal function. We therefore compared QUIN/TRP ratios in striatum to

corpus callosum levels of APP and found that QUIN/TRP ratios strongly correlated with APP (r = 0.770; *P* = 0.013; Fig. 4d). Thus, overall the QUIN/TRP ratio in the brain was a sensitive marker for a variety of neuropathological changes including encephalitis severity as well as more quantitative measures such as macrophage/microglial activation, viral load, and neuronal damage, several of which are also surrogate markers for motor aberrations during HIV/SIV infection.

cART attenuates, but does not abolish, KP activation in striatum of infected animals

Elevations in KP metabolites in CSF and plasma are often incompletely resolved by cART in patients and in animal models of HIV infection (Gendelman et al. 1998; Jenabian et al. 2013; Chen et al. 2014). However, levels of KP metabolites in brain tissue following cART have not been reported. To test the efficacy of cART on the normalization of KP activation in the CNS, we examined the levels of TRP and KP metabolites in the striatum and CSF of animals whose CSF and plasma viral loads had been suppressed for approximately 100 days with a 4-drug cART regimen. In this model, cART-treated animals had no detectable viral RNA in striatum at euthanasia and did not have encephalitis, though integrated viral DNA was still present (Zink et al. 2010).

In the present study, we tested whether levels of KP metabolites in the cART animals were normalized to uninfected control levels. Striatal levels of TRP in the cART-treated animals were not significantly different from uninfected controls (Fig. 5a). In contrast, all of the metabolites in cART-treated animals remained significantly higher than uninfected controls (KYN: *P* = 0.0007; 3HK: *P* = 0.028; QUIN: *P* = 0.003; KYN/TRP ratios: *P* = 0.0007; QUIN/TRP ratios: *P* = 0.001; Fig. 5b–f). Thus, striatal KP metabolites remained elevated despite suppression of active viral replication in the brain.

CSF QUIN/TRP ratios correlate with brain QUIN/TRP ratios

We next analyzed the levels of metabolites in the CSF of the cART-treated animals at three suppressed time points between 100 and 175 days p.i., including a sample taken at euthanasia (Fig. 6a). Consistent with the fact that the cART animals did not display any signs of encephalitis, their median CSF levels of TRP and KP metabolites terminally were indistinguishable from their matched, pre-infection values (Fig. 6b–g). However, one animal in particular (cART 2, open square) consistently displayed a deficit in CSF TRP levels and had the highest changes in CSF QUIN (Fig. 6e) and QUIN/TRP ratios (Fig. 6g). Furthermore, this animal also displayed elevated IL-6 and MCP-1 in the CSF during this period of viral suppression (Fig. S2c, d), and had the highest striatal levels of QUIN and QUIN/TRP ratios within the cART group. These data led us to hypothesize that CSF levels of KP metabolites would correlate with brain levels even in animals on cART.

We therefore compared individually matched terminal CSF and striatal concentrations of TRP and KP metabolites in thirteen SIV-infected macaques, including the eight untreated macaques from Figure 2 and the five cART-treated macaques from Figure 6. Indeed, all of the analytes with the exception of 3HK displayed a strong positive correlation between terminal CSF and terminal striatal levels (Fig. 7*B-F*; TRP: r = 0.582; *P* = 0.040; KYN: r = 0.714; *P* = 0.008; 3HK: r = 0.352; *P* = 0.239; QUIN: r = 0.940; *P* < 0.0001; KYN/TRP ratio:

r = 0.703; *P* = 0.009; QUIN/TRP ratio: r = 0.769; *P* = 0.003), cementing the value of CSF analytes such as QUIN/TRP as a surrogate measure for KP activation in the brain.

Serotonin decreases during acute and chronic infection

We also measured striatal serotonin levels in the macaques because increased turnover of TRP via the KP may reduce the pool of TRP available for serotonin synthesis. Striatal serotonin levels were significantly decreased during acute (*P* = 0.006 at the nadir on day 14 p.i.; Fig. 8a) and chronic infection (*P* = 0.015; Fig. 8a) in the SIV-infected macaques. However, striatal serotonin levels did not significantly differ by encephalitis severity (Fig. 8a), nor did they correlate with KP activation as measured by striatal QUIN/TRP ratios (Fig. S3).

Finally, although all five cART-treated animals displayed serotonin levels below the median of uninfected controls, they were not significantly different from uninfected controls (*P* = 0.096; Fig. 8b), suggesting that cART was at least partially protective against serotonin losses.

Discussion

Key findings from our study include 1) identification of CSF QUIN/TRP ratios as a novel, early predictive biomarker of neurological disease, 2) demonstration of serotonin losses that coincide but do not correlate with KP upregulation in the brain, and 3) incomplete normalization of KP activation in the brain despite viral suppression under cART. These results suggest that the KP may contribute to HIV-associated motor/cognitive disorders and depression even in individuals successfully treated with cART.

While no biomarker as of yet has proven to be clinically useful at predicting or diagnosing HIV-associated neurological disease, CSF levels of QUIN, MCP-1, and IL-6 are frequently cited as top biomarker candidates (Brew and Letendre 2008). QUIN in particular has been shown to differentiate between HIV-infected individuals with or without dementia (Heyes et al. 1991), with or without functional impairments in motor-skill learning and reaction time (Martin et al. 1993), as well as SIV-infected macaques with or without encephalitis (Heyes et al. 1992a). However, an ideal biomarker for HIV-associated neurological disorders should identify at-risk patients *before* the onset of potentially irreversible neurological changes and should differentiate between milder forms of disease.

By normalizing QUIN to TRP levels we generated a novel biomarker that not only represents cumulative KP activation through the neurotoxic QUIN axis, but also predicted development of encephalitis by day 28 p.i., a remarkably early time point during the asymptomatic phase of infection in our model. In contrast, QUIN, MCP-1, and IL-6 did not reach significance until day 42 p.i. Importantly, the CSF QUIN/TRP ratio was sensitive at detecting even minor neurological changes: 4 of the 5 cART-treated animals had no elevations in CSF QUIN/TRP ratios in line with the fact that they had no detectable neurological disease (Fig. 6), while all of the untreated animals that developed mild encephalitis displayed corresponding small elevations in CSF QUIN/TRP ratios. Additionally, CSF QUIN/TRP ratios strongly correlated with brain QUIN/TRP ratios,

regardless of encephalitis or treatment status, suggesting that the CSF QUIN/TRP ratio may be useful as a biomarker for predicting encephalitis development prior to treatment initiation as well as for monitoring the development of neurological disease under cART. However, a major hurdle preventing the broader implementation of QUIN/TRP ratios as a clinical biomarker is the technical difficulty of measuring QUIN by GC/MS, the gold standard technique for this metabolite. Novel approaches, such as the HPLC method reported by Raison *et al.* that utilized recombinant enzymes to generate a fluorescent product from endogenous QUIN (Raison et al. 2010) may be necessary in order to make QUIN/TRP measurements more accessible. In spite of these technical challenges, our findings provide impetus for future clinical studies using the CSF QUIN/TRP ratio as a biomarker for neurological disease.

Given the central role of activated macrophages/microglia in the pathogenesis of HIV-associated neurological disorders, it is not surprising that a marker involved in the recruitment of macrophages to the brain (MCP-1) and markers secreted by macrophages/microglia in the brain (QUIN, IL-6) have emerged as prominent biomarker candidates. In the present study, striatal QUIN/TRP ratios strongly correlated with markers of macrophage/microglial activation (CD68, MHC Class II) as well as striatal SIV RNA and the neuronal damage marker APP, supporting a direct link between accumulation of neurological damage over time and activation of macrophages/microglia, the long-lived cellular reservoirs of virus in the brain. This connection was also visible in the cART-treated animals, where the lone animal that displayed residual elevations in QUIN/TRP ratios also had elevations in MCP-1 and IL-6 despite its viremia being well suppressed.

In general, KYN, 3HK, and QUIN levels were all significantly elevated in the brain during acute and chronic infection and were highest in the animals with the most severe encephalitis. We also found that upstream enzymes in the KP, *IDO1*, *KMO*, and *KYNU*, were transcriptionally upregulated during infection in striatum, particularly in animals with moderate to severe encephalitis. In contrast, the downstream enzymes *HAAO* and *QPRT* were unchanged. These transcriptional findings in striatum are in excellent agreement with a previous report showing that the activity levels of the enzymes IDO1, KMO, and KYNU, but not HAAO, are increased in lesioned cortex during retroviral infections in macaques (Heyes et al. 1998), and suggest a strong role for transcriptional upregulation of upstream KP enzymes during inflammation. The fact that *QPRT*, the enzyme responsible for clearance of QUIN, was unchanged during infection also helps to explain why QUIN accumulates to such high levels in the brain and may represent a therapeutic target whose induction may be protective in HAND. Determining the cellular localization of KP enzymes within the brain remains an important future direction, although previous studies have consistently highlighted macrophages and microglia as the most important cerebral sources of IDO expression and quinolinic acid production in humans and in rhesus macaques, while human astrocytes and neurons have been shown to be deficient in critical KP enzymes (KMO for astrocytes, KMO and KYNU for neurons) (Burudi et al. 2002; Guillemin et al. 2005). Such complexities in KP enzyme expression the brain have yet to be confirmed in pigtailed macaques, but *in vitro* studies comparing KP enzyme expression in human versus rhesus,

pigtailed, and cynomolgus macaque macrophages have suggested nearly identical KP regulation across these primate species (Lim et al. 2013).

Inversely paralleling the changes in KP metabolites in the brain, striatal serotonin levels were significantly decreased during both the acute (day 14 p.i.) and chronic phases of infection. These findings confirm and expand upon a previous report that showed a deficit in serotonin levels in patients who had progressed to AIDS, though that study was confounded by the presence of opportunistic infections in the CNS and variable postmortem delays (Reynolds and Sardar 1996). Our carefully controlled pigtailed macaque model is devoid of such confounding factors and therefore provides strong evidence that serotonin stores are in fact depleted in brain tissue during SIV/HIV infection. Such deficits may contribute to the incidence of mood disorders such as depression that are commonly seen in HIV-infected patients (Heaton et al. 2010; Ances and Ellis 2007; Chibanda et al. 2014). Others have reported modest associations between KP activation and depression, both in hepatitis C-infected individuals treated with IFNα/ribavirin therapy (Raison et al. 2010) as well as in HIV-infected individuals before and during cART (Martinez et al. 2014). However, we did not find a significant correlation between QUIN/TRP ratios and striatal serotonin levels in our chronically infected animals. Overall, these data suggest that other factors in addition to KP activation likely contribute to the dysregulation of serotonin during infection, while neither KP activation nor serotonin deficits can account for the onset of all depressive disorders. Importantly, serotonin losses during acute infection were recovered by day 21 p.i. in our model, and cART-treated animals did not have significantly lower levels of serotonin terminally compared to uninfected controls, suggesting that losses in serotonin are at least partially reversible.

Although we expected TRP levels to be reduced in the brain as a consequence of KP activation, we found that striatal TRP levels were not significantly downregulated at any stage of SIV infection. This was in contrast to the CSF, in which rapid and sustained deficits in TRP were observed. These data suggest that cells within the brain maintain their intracellular TRP levels during KP activation by depleting extracellular stores of TRP as evidenced by reduced TRP in the CSF. However, the fact that terminal CSF and striatal TRP levels still positively correlated with one another, and the fact that TRP levels in the brain separated by encephalitis severity during chronic infection despite the overall lack of change, suggests that KP activation does have a biological effect on TRP reservoirs in the brain even if it is not a statistically significant one.

Finally, we found that cART-treated animals displayed a modest but significant elevation in all KP metabolites in brain tissue despite the successful suppression of peripheral and CNS viral replication. In addition, one animal had persistent, low-level elevations in CSF QUIN/TRP ratios. While the cART-treated animals did not display any pathological signs of neurological disease and their striatal QUIN levels (median 277 nM) were not sufficient to induce acute neuronal excitotoxicity, chronic exposure of striatal neurons to sub-micromolar levels of QUIN has been reported to cause cytoskeletal changes indicative of NMDA receptor-mediated excitotoxicity (Whetsell and Schwarcz 1989; Kerr et al. 1998). Additionally, the striatum is more susceptible to QUIN-mediated excitotoxicity than other brain regions (Schwarcz and Kohler 1983), and low levels of QUIN can synergize with 3HK

neurotoxicity (Guidetti and Schwarcz 1999). Neurons near foci of viral replication or macrophage/microglial activation would likely be exposed to even higher levels of these metabolites, suggesting a potential pathogenic role for both 3HK and QUIN under cART.

In conclusion, our findings highlight the QUIN/TRP ratio as a sensitive, early predictive biomarker of inflammatory neurological disease. This measure may also be useful for monitoring neurological status during treatment, particularly when used in conjunction with other markers such as MCP-1, IL-6, etc. Due to the limitations of cognitive testing in macaques, follow-up evaluations of QUIN/TRP ratios in patient cohorts will be essential but are highly likely to succeed given the results of studies with QUIN alone in patients (Heyes et al. 1989; Heyes et al. 1998). Additionally, our data on serotonin, TRP, and the KP provide mechanistic clues as to why not all patients with neurocognitive deficits develop depression. Finally, our studies emphasize the need for targeted inhibition of the KP alongside cART or a better understanding of the efficacy of different cART regimens in controlling residual CNS immune activation.

Supplementary Material

Refer to Web version on PubMed Central for supplementary material.

Acknowledgments

## References

Ances BM, Ellis RJ. Dementia and neurocognitive disorders due to HIV-1 infection. Seminars in neurology. 2007; 27(1):86–92. [PubMed: 17226745]

Brew BJ, Letendre SL. Biomarkers of HIV related central nervous system disease. International review of psychiatry. 2008; 20(1):73–88. [PubMed: 18240064]

Burudi EM, Marcondes MC, Watry DD, Zandonatti M, Taffe MA, Fox HS. Regulation of indoleamine 2,3-dioxygenase expression in simian immunodeficiency virus-infected monkey brains. J Virol. 2002; 76(23):12233–12241. [PubMed: 12414962]

Chen J, Shao J, Cai R, Shen Y, Zhang R, Liu L, Qi T, Lu H. Anti-retroviral therapy decreases but does not normalize indoleamine 2,3-dioxygenase activity in HIV-infected patients. PLoS One. 2014; 9(7):e100446. [PubMed: 24983463]

Chibanda D, Benjamin L, Weiss HA, Abas M. Mental, neurological, and substance use disorders in people living with HIV/AIDS in low- and middle-income countries. J Acquir Immune Defic Syndr. 2014; 67(Suppl 1):S54–S67. [PubMed: 25117961]

Clements JE, Mankowski JL, Gama L, Zink MC. The accelerated simian immunodeficiency virus macaque model of human immunodeficiency virus-associated neurological disease: from mechanism to treatment. J Neurovirol. 2008; 14(4):309–317. [PubMed: 18780232]

Dantzer R, O'Connor JC, Lawson MA, Kelley KW. Inflammation-associated depression: from serotonin to kynurenine. Psychoneuroendocrinology. 2011; 36(3):426–436. [PubMed: 21041030]

Del Guerra FB, Fonseca JL, Figueiredo VM, Ziff EB, Konkiewitz EC. Human immunodeficiency virus-associated depression: contributions of immuno-inflammatory, monoaminergic, neurodegenerative, and neurotrophic pathways. J Neurovirol. 2013; 19(4):314–327. [PubMed: 23868513]

Dinoso JB, Rabi SA, Blankson JN, Gama L, Mankowski JL, Siliciano RF, Zink MC, Clements JE. A simian immunodeficiency virus-infected macaque model to study viral reservoirs that persist during highly active antiretroviral therapy. J Virol. 2009; 83(18):9247–9257. [PubMed: 19570871]

Fuchs D, Forsman A, Hagberg L, Larsson M, Norkrans G, Reibnegger G, Werner ER, Wachter H. Immune activation and decreased tryptophan in patients with HIV-1 infection. J Interferon Res. 1990; 10(6):599–603. [PubMed: 2128302]

Gendelman HE, Zheng J, Coulter CL, Ghorpade A, Che M, Thylin M, Rubocki R, Persidsky Y, Hahn F, Reinhard J Jr. Swindells S. Suppression of inflammatory neurotoxins by highly active antiretroviral therapy in human immunodeficiency virus-associated dementia. J Infect Dis. 1998; 178(4):1000–1007. [PubMed: 9806027]

Guidetti P, Schwarcz R. 3-Hydroxykynurenine potentiates quinolinate but not NMDA toxicity in the rat striatum. Eur J Neurosci. 1999; 11(11):3857–3863. [PubMed: 10583474]

Guillemin GJ, Kerr SJ, Smythe GA, Smith DG, Kapoor V, Armati PJ, Croitoru J, Brew BJ. Kynurenine pathway metabolism in human astrocytes: a paradox for neuronal protection. J Neurochem. 2001; 78(4):842–853. [PubMed: 11520905]

Guillemin GJ, Smythe G, Takikawa O, Brew BJ. Expression of indoleamine 2,3-dioxygenase and production of quinolinic acid by human microglia, astrocytes, and neurons. Glia. 2005; 49(1):15–23. [PubMed: 15390107]

Heaton RK, Clifford DB, Franklin DR Jr. Woods SP, Ake C, Vaida F, Ellis RJ, Letendre SL, Marcotte TD, Atkinson JH, Rivera-Mindt M, Vigil OR, Taylor MJ, Collier AC, Marra CM, Gelman BB, McArthur JC, Morgello S, Simpson DM, McCutchan JA, Abramson I, Gamst A, Fennema-Notestine C, Jernigan TL, Wong J, Grant I. HIV-associated neurocognitive disorders persist in the era of potent antiretroviral therapy: CHARTER Study. Neurology. 2010; 75(23):2087–2096. [PubMed: 21135382]

Heyes MP, Brew BJ, Martin A, Price RW, Salazar AM, Sidtis JJ, Yergey JA, Mouradian MM, Sadler AE, Keilp J, et al. Quinolinic acid in cerebrospinal fluid and serum in HIV-1 infection: relationship to clinical and neurological status. Ann Neurol. 1991; 29(2):202–209. [PubMed: 1826418]

Heyes MP, Jordan EK, Lee K, Saito K, Frank JA, Snoy PJ, Markey SP, Gravell M. Relationship of neurologic status in macaques infected with the simian immunodeficiency virus to cerebrospinal fluid quinolinic acid and kynurenic acid. Brain Res. 1992a; 570(1-2):237–250. [PubMed: 1535532]

Heyes MP, Rubinow D, Lane C, Markey SP. Cerebrospinal fluid quinolinic acid concentrations are increased in acquired immune deficiency syndrome. Ann Neurol. 1989; 26(2):275–277. [PubMed: 2528321]

Heyes MP, Saito K, Crowley JS, Davis LE, Demitrack MA, Der M, Dilling LA, Elia J, Kruesi MJ, Lackner A, et al. Quinolinic acid and kynurenine pathway metabolism in inflammatory and non-inflammatory neurological disease. Brain. 1992b; 115(Pt 5):1249–1273. [PubMed: 1422788]

Heyes MP, Saito K, Lackner A, Wiley CA, Achim CL, Markey SP. Sources of the neurotoxin quinolinic acid in the brain of HIV-1-infected patients and retrovirus-infected macaques. FASEB J. 1998; 12(10):881–896. [PubMed: 9657528]

Jenabian MA, Patel M, Kema I, Kanagaratham C, Radzioch D, Thebault P, Lapointe R, Tremblay C, Gilmore N, Ancuta P, Routy JP. Distinct Tryptophan Catabolism and Th17/Treg Balance in HIV Progressors and Elite Controllers. PLoS One. 2013; 8(10):e78146. [PubMed: 24147117]

Kerr SJ, Armati PJ, Guillemin GJ, Brew BJ. Chronic exposure of human neurons to quinolinic acid results in neuronal changes consistent with AIDS dementia complex. AIDS. 1998; 12(4):355–363. [PubMed: 9520164]

Kumar AM, Berger JR, Eisdorfer C, Fernandez JB, Goodkin K, Kumar M. Cerebrospinal fluid 5-hydroxytryptamine and 5-hydroxyindoleacetic acid in HIV-1 infection. Neuropsychobiology. 2001; 44(1):13–18. [PubMed: 11408787]

Larsson M, Hagberg L, Norkrans G, Forsman A. Indole amine deficiency in blood and cerebrospinal fluid from patients with human immunodeficiency virus infection. J Neurosci Res. 1989; 23(4): 441–446. [PubMed: 2475644]

Lim CK, Yap MM, Kent SJ, Gras G, Samah B, Batten JC, De Rose R, Heng B, Brew BJ, Guillemin GJ. Characterization of the kynurenine pathway and quinolinic Acid production in macaque macrophages. International journal of tryptophan research : IJTR. 2013; 6:7–19. [PubMed: 23761975]

Mankowski JL, Queen SE, Clements JE, Zink MC. Cerebrospinal fluid markers that predict SIV CNS disease. J Neuroimmunol. 2004; 157(1-2):66–70. [PubMed: 15579282]

Mankowski JL, Queen SE, Tarwater PM, Fox KJ, Perry VH. Accumulation of beta-amyloid precursor protein in axons correlates with CNS expression of SIV gp41. J Neuropathol Exp Neurol. 2002; 61(1):85–90. [PubMed: 11829347]

Martin A, Heyes MP, Salazar AM, Law WA, Williams J. Impaired motor-skill learning, slowed reaction time, and elevated cerebrospinal-fluid quinolinic acid in a subgroup of HIV-infected individuals. Neuropsychology. 1993; 7(2):149–157.

Martinez P, Tsai AC, Muzoora C, Kembabazi A, Weiser SD, Huang Y, Haberer JE, Martin JN, Bangsberg DR, Hunt PW. Reversal of the Kynurenine pathway of tryptophan catabolism may improve depression in ART-treated HIV-infected Ugandans. J Acquir Immune Defic Syndr. 2014; 65(4):456–462. [PubMed: 24220289]

McArthur JC, Brew BJ, Nath A. Neurological complications of HIV infection. Lancet Neurol. 2005; 4(9):543–555. [PubMed: 16109361]

Meulendyke KA, Ubaida-Mohien C, Drewes JL, Liao Z, Gama L, Witwer KW, Graham DR, Zink MC. Elevated brain monoamine oxidase activity in SIV and HIV neurological disease. J Infect Dis. 2014

Notarangelo FM, Wu HQ, Macherone A, Graham DR, Schwarcz R. Gas chromatography/tandem mass spectrometry detection of extracellular kynurenine and related metabolites in normal and lesioned rat brain. Anal Biochem. 2012; 421(2):573–581. [PubMed: 22239963]

Okuda S, Nishiyama N, Saito H, Katsuki H. 3-Hydroxykynurenine, an endogenous oxidative stress generator, causes neuronal cell death with apoptotic features and region selectivity. J Neurochem. 1998; 70(1):299–307. [PubMed: 9422375]

Raison CL, Dantzer R, Kelley KW, Lawson MA, Woolwine BJ, Vogt G, Spivey JR, Saito K, Miller AH. CSF concentrations of brain tryptophan and kynurenines during immune stimulation with IFN-alpha: relationship to CNS immune responses and depression. Molecular psychiatry. 2010; 15(4):393–403. [PubMed: 19918244]

Reynolds GP, Sardar AM. 5-Hydroxytryptamine deficits in the caudate nucleus in AIDS. AIDS. 1996; 10(11):1303–1304. [PubMed: 8883602]

Robertson KR, Smurzynski M, Parsons TD, Wu K, Bosch RJ, Wu J, McArthur JC, Collier AC, Evans SR, Ellis RJ. The prevalence and incidence of neurocognitive impairment in the HAART era. AIDS. 2007; 21(14):1915–1921. [PubMed: 17721099]

Ruhe HG, Mason NS, Schene AH. Mood is indirectly related to serotonin, norepinephrine and dopamine levels in humans: a meta-analysis of monoamine depletion studies. Molecular psychiatry. 2007; 12(4):331–359. [PubMed: 17389902]

Sardar AM, Bell JE, Reynolds GP. Increased concentrations of the neurotoxin 3-hydroxykynurenine in the frontal cortex of HIV-1-positive patients. J Neurochem. 1995; 64(2):932–935. [PubMed: 7830088]

Schwarcz R, Köhler C. Differential vulnerability of central neurons of the rat to quinolinic acid. Neurosci Lett. 1983; 38(1):85–90. [PubMed: 6225037]

Schwarcz R, Whetsell WO Jr. Mangano RM. Quinolinic acid: an endogenous metabolite that produces axon-sparing lesions in rat brain. Science. 1983; 219(4582):316–318. [PubMed: 6849138]

Smith KA, Fairburn CG, Cowen PJ. Relapse of depression after rapid depletion of tryptophan. Lancet. 1997; 349(9056):915–919. [PubMed: 9093253]

Weed MR, Hienz RD, Brady JV, Adams RJ, Mankowski JL, Clements JE, Zink MC. Central nervous system correlates of behavioral deficits following simian immunodeficiency virus infection. J Neurovirol. 2003; 9(4):452–464. [PubMed: 12907390]

Whetsell WO Jr. Schwarcz R. Prolonged exposure to submicromolar concentrations of quinolinic acid causes excitotoxic damage in organotypic cultures of rat corticostriatal system. Neurosci Lett. 1989; 97(3):271–275. [PubMed: 2524015]

Witwer KW, Gama L, Li M, Bartizal CM, Queen SE, Varrone JJ, Brice AK, Graham DR, Tarwater PM, Mankowski JL, Zink MC, Clements JE. Coordinated regulation of SIV replication and immune responses in the CNS. PLoS One. 2009; 4(12):e8129. [PubMed: 20019816]

Zink MC, Brice AK, Kelly KM, Queen SE, Gama L, Li M, Adams RJ, Bartizal C, Varrone J, Rabi SA, Graham DR, Tarwater PM, Mankowski JL, Clements JE. Simian immunodeficiency virus-infected macaques treated with highly active antiretroviral therapy have reduced central nervous system viral replication and inflammation but persistence of viral DNA. J Infect Dis. 2010; 202(1):161–170. [PubMed: 20497048]

Zink MC, Suryanarayana K, Mankowski JL, Shen A, Piatak M Jr. Spelman JP, Carter DL, Adams RJ, Lifson JD, Clements JE. High viral load in the cerebrospinal fluid and brain correlates with severity of simian immunodeficiency virus encephalitis. J Virol. 1999; 73(12):10480–10488. [PubMed: 10559366]
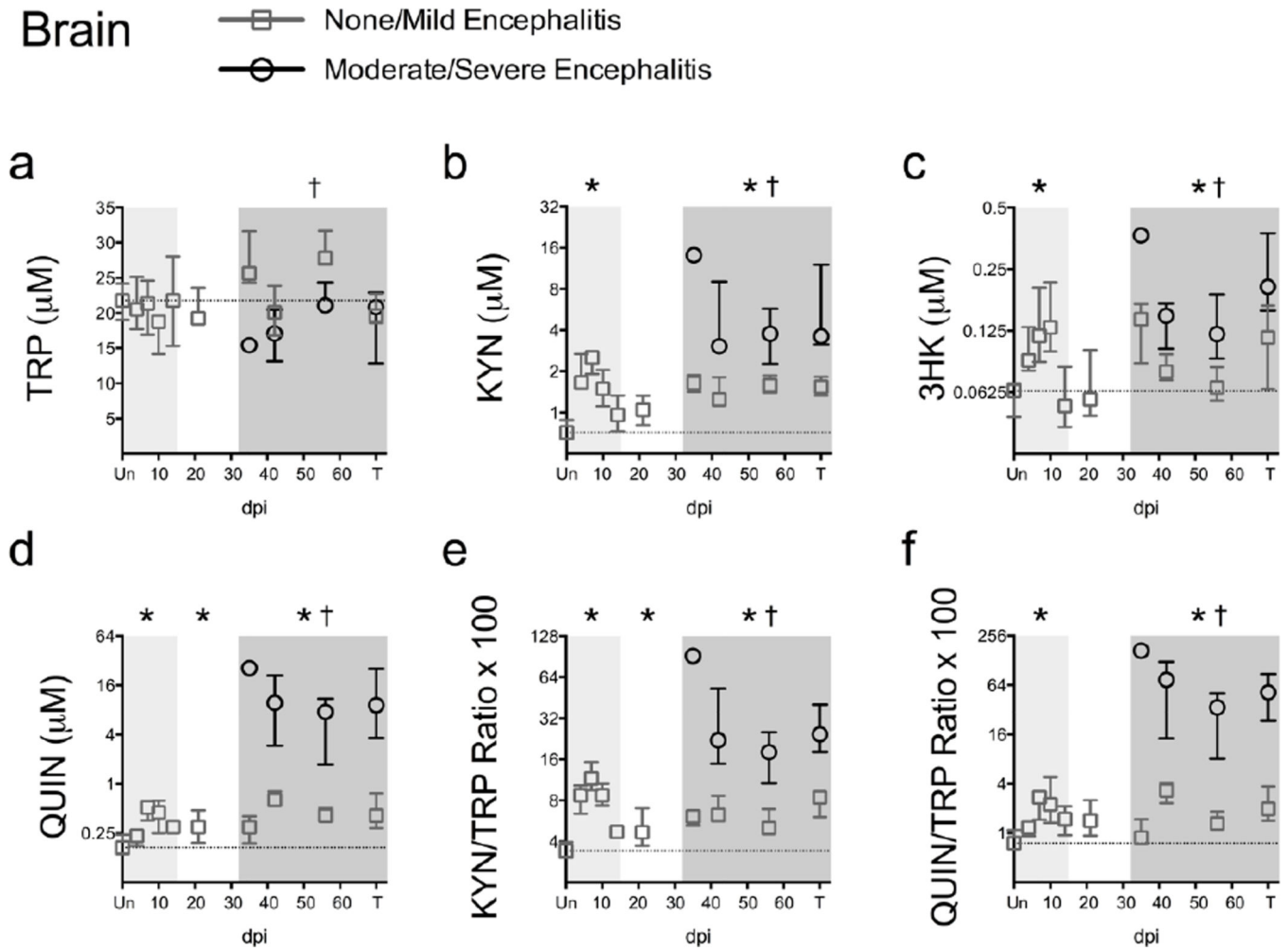
Fig. 1.
Striatal KP metabolites increase biphasically during SIV infection. TRP (**a**), KYN (**b**), 3HK (**c**), QUIN (**d**), KYN/TRP ratios (**e**), and QUIN/TRP ratios (**f**) were measured in perfused striatum from 79 animals euthanized at various time points throughout infection (6 – 13 animals per timepoint). "Un" represents uninfected animals; "T" represents animals euthanized at 84 days p.i. or due to terminal disease criteria. Medians and interquartile ranges are depicted for animals that had none/mild (grey squares) and moderate/severe (black circles) encephalitis at euthanasia. The dotted line represents the median of uninfected animals. Light grey shading represents the acute phase of infection (0–14 dpi), and dark grey shading represents the chronic phase of infection (35 dpi) in our model. Asterisks (*) indicate whether the peak during acute infection, or the total values during asymptomatic or chronic infection, were significantly different ($P < 0.05$) from uninfected controls by Mann-Whitney U test. Crosses (†) represent metabolites that were significantly different ($P < 0.05$) between the two encephalitis outcomes during chronic infection by Mann-Whitney U test.
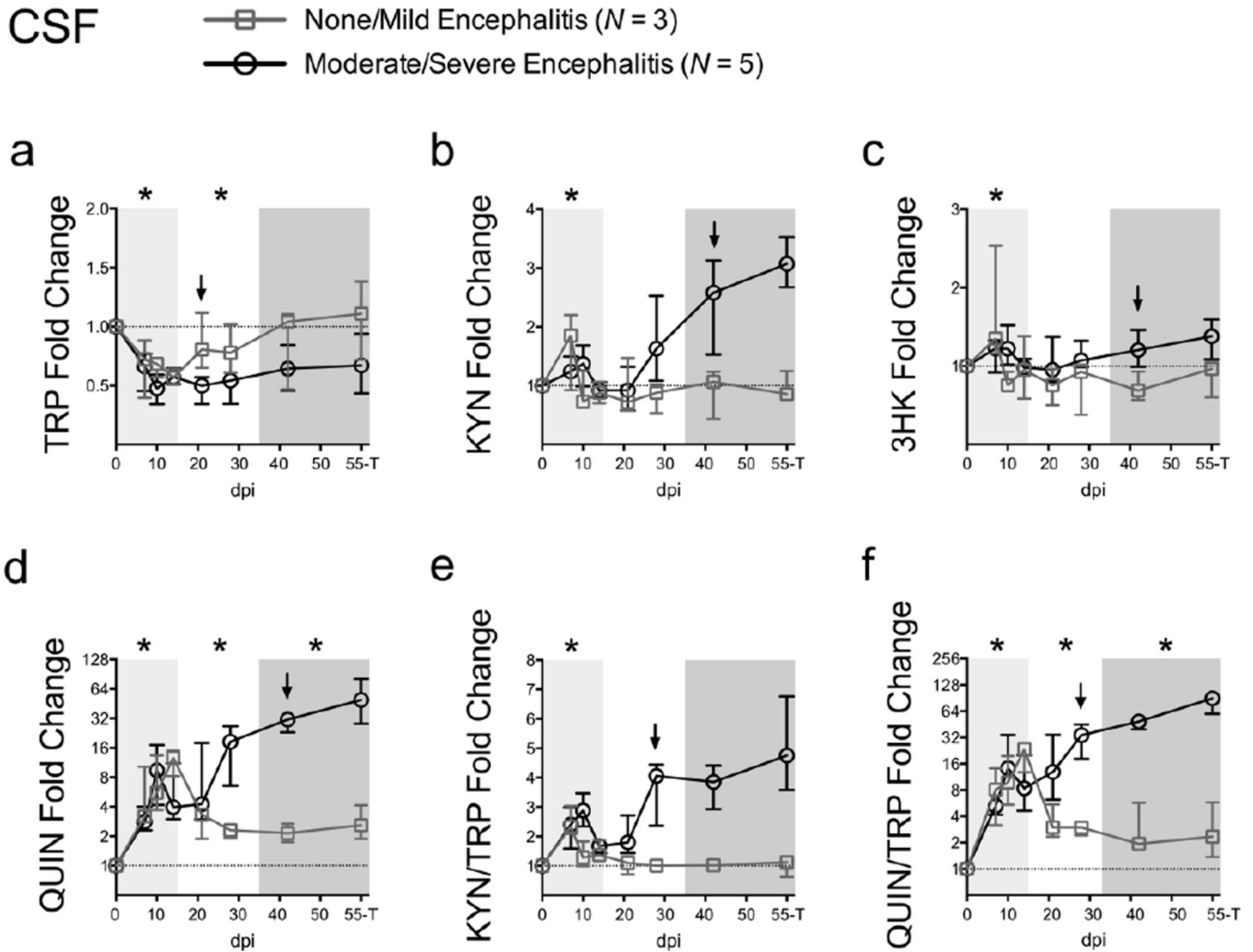
Fig. 2.
CSF QUIN/TRP ratios are an early predictor of encephalitis development. TRP (**a**), KYN (**b**), 3HK (**c**), QUIN (**d**), KYN/TRP ratios (**e**), and QUIN/TRP ratios (**f**) were analyzed in CSF sampled longitudinally from 3 animals with no/mild encephalitis at euthanasia (grey squares) and 5 with moderate/severe encephalitis at euthanasia (black circles). The "55-T" timepoint on the x-axis of each graph represents the day 56 p.i. time point for all animals except for one rapid progressor, whose terminal disease time point at day 50 p.i. is shown instead. Data are plotted as the median fold change +/− interquartile ranges over the average of 3 pre-infection CSF draws from each animal (dotted line). Light grey shading represents the acute phase of infection (0–14 dpi), and dark grey shading represents the chronic phase of infection (35 dpi) in our model. Asterisks (*) indicate whether the peak for each animal during acute infection, or median values for each animal during asymptomatic and chronic infection, were significantly different ($P < 0.05$) from their respective pre-infection values by Wilcoxon signed rank test. Arrows represent the earliest time point at which metabolite levels were significantly different ($P < 0.05$) between the two encephalitis outcomes by Mann-Whitney U test.
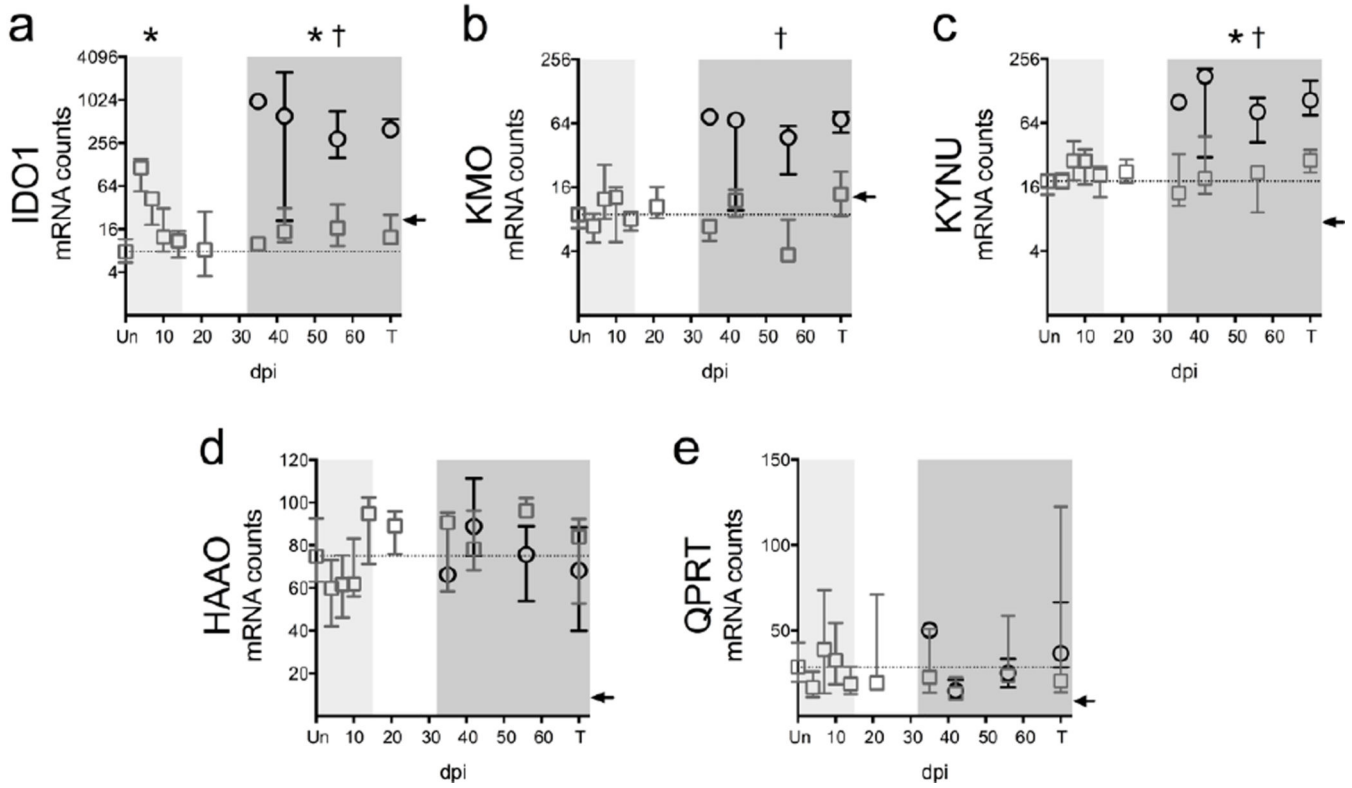
Fig. 3.
Expression of upstream but not downstream KP enzymes increases during infection in striatum. (**a** to **e**) The mRNA expression of 5 KP enzymes was analyzed in perfused striatum from 79 animals using the Nanostring nCounter system. "Un" represents uninfected animals; "T" represents SIV-infected animals euthanized at 84 days p.i. or due to terminal disease criteria. Medians and interquartile ranges are depicted for animals that had none/mild (grey squares) and moderate/severe (black circles) encephalitis at euthanasia. Light grey shading represents the acute phase of infection (0–14 dpi), and dark grey shading represents the chronic phase of infection (35 dpi) in our model. The dotted lines designate the medians of uninfected controls. The black arrow on each graph represents the gene-specific, low-confidence thresholds as determined by the average plus 2 standard deviations of bacteriophage RNA that should not cross-hybridize with Nanostring probes. Asterisks (*) indicate whether the peak during acute infection, or the total values during asymptomatic or chronic infection, were significantly different ($P < 0.05$) from uninfected controls by Mann-Whitney U test. Crosses (†) represent transcripts that were significantly different ($P < 0.05$) between the two encephalitis outcomes during chronic infection by Mann-Whitney U test.
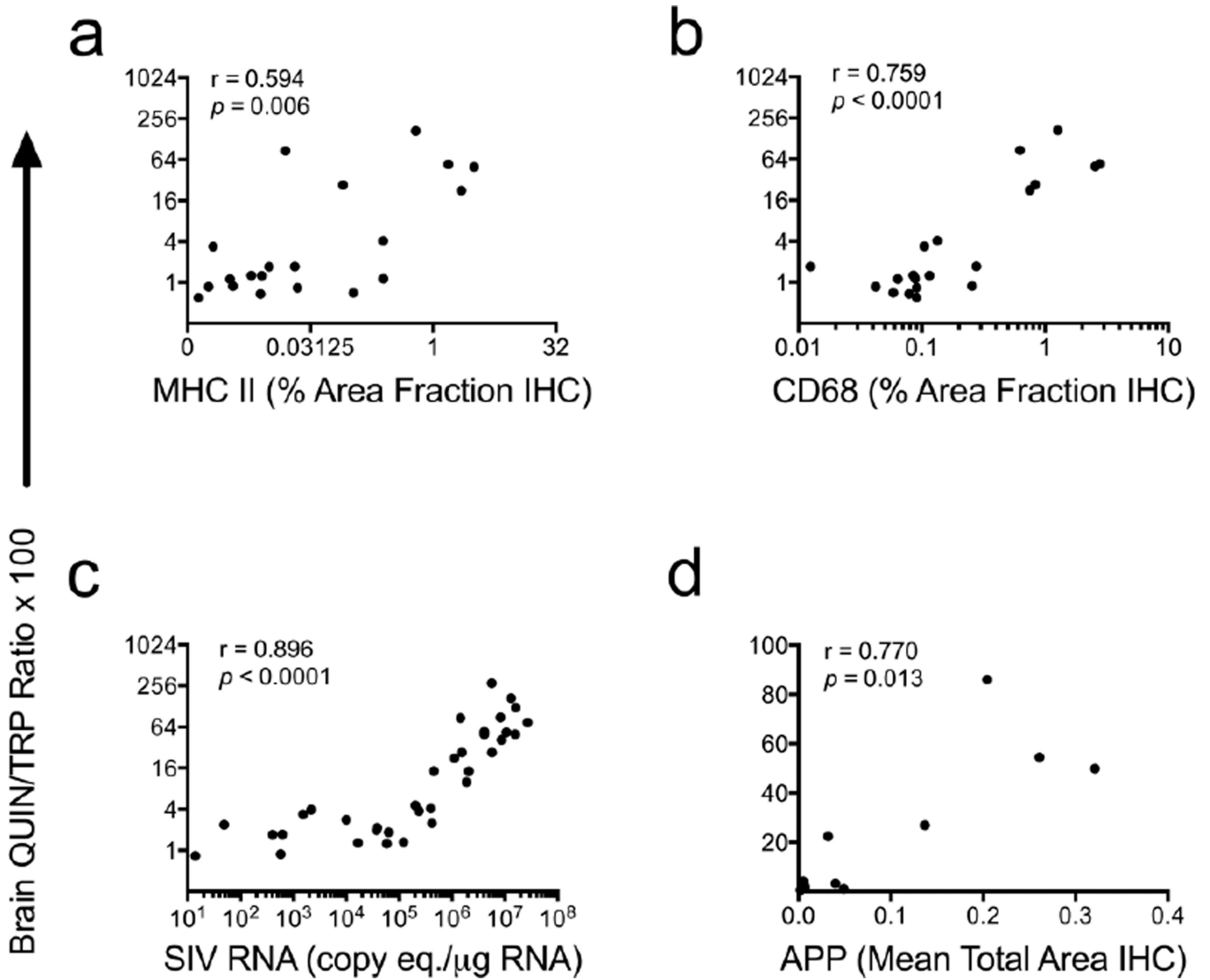
Fig. 4.

Striatal QUIN/TRP ratios correlate with markers of neuropathogenesis in chronically infected animals. QUIN/TRP ratios in striatum from chronically infected animals (35 dpi) were measured and compared against markers and inducers of neuropathogenesis. (**a** and **b**) Correlations of striatal QUIN/TRP ratios versus markers of macrophage/ microglial activation (MHC II, CD68), measured by immunohistochemistry (IHC) in subcortical white matter adjacent to striatum (N = 20 animals). (**c**) Correlation of striatal QUIN/TRP ratios versus striatal SIV viral RNA (N = 37 animals). (**d**) Correlation of QUIN/TRP ratios versus amyloid precursor protein (APP), a marker of neuronal axon damage, as measured by IHC in corpus callosum (N = 10 animals). All statistical analyses are Spearman's rank correlations.
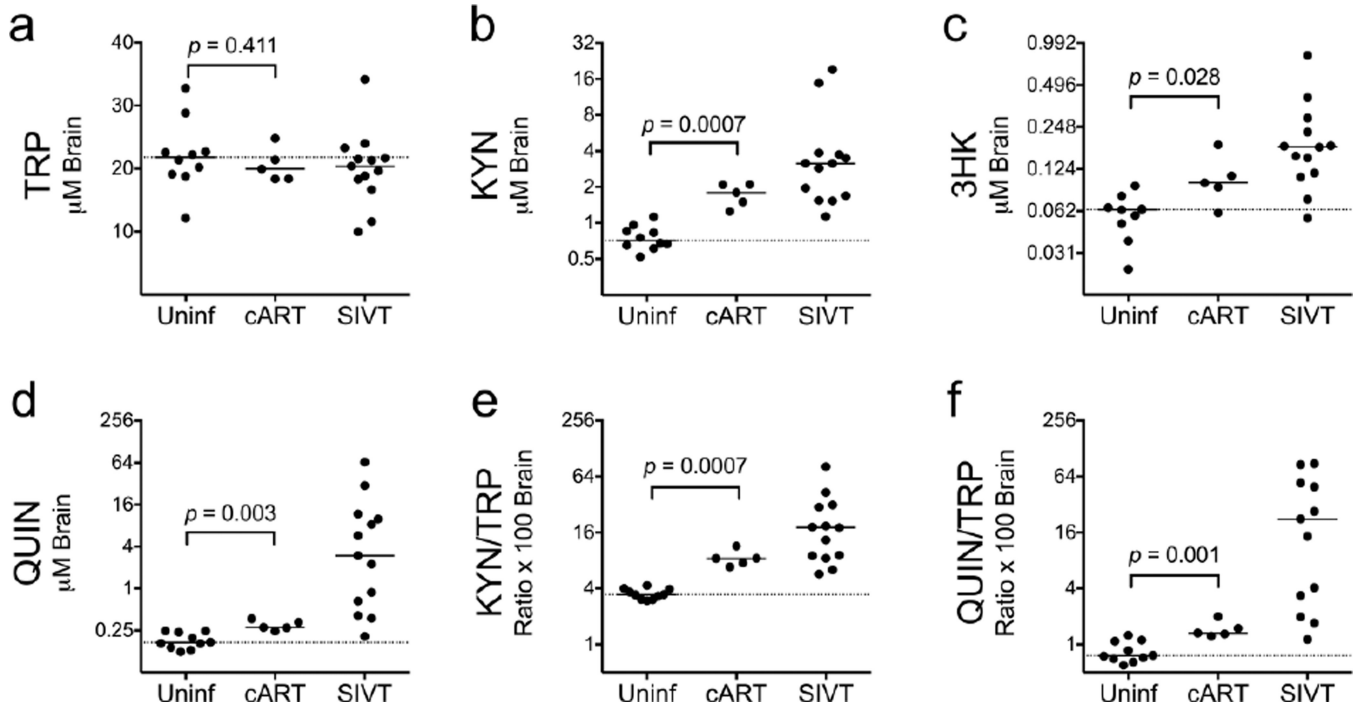
Fig. 5.
cART does not fully protect against KP activation in the brain. Levels of TRP (**a**), KYN (**b**), 3HK (**c**), QUIN (**d**), KYN/TRP ratios (**e**), and QUIN/TRP ratios (**f**) were measured in perfused striatum of 10 uninfected controls (Uninf), 13 SIV-infected, untreated animals that were euthanized with terminal disease (SIVT), and 5 SIV-infected animals treated with cART starting at day 12 p.i. that were euthanized after approximately 100 days of viremia suppression (161–175 days p.i.). Horizontal bars represent medians. The dotted lines represent the medians of uninfected controls. Data were analyzed by Mann-Whitney U test.
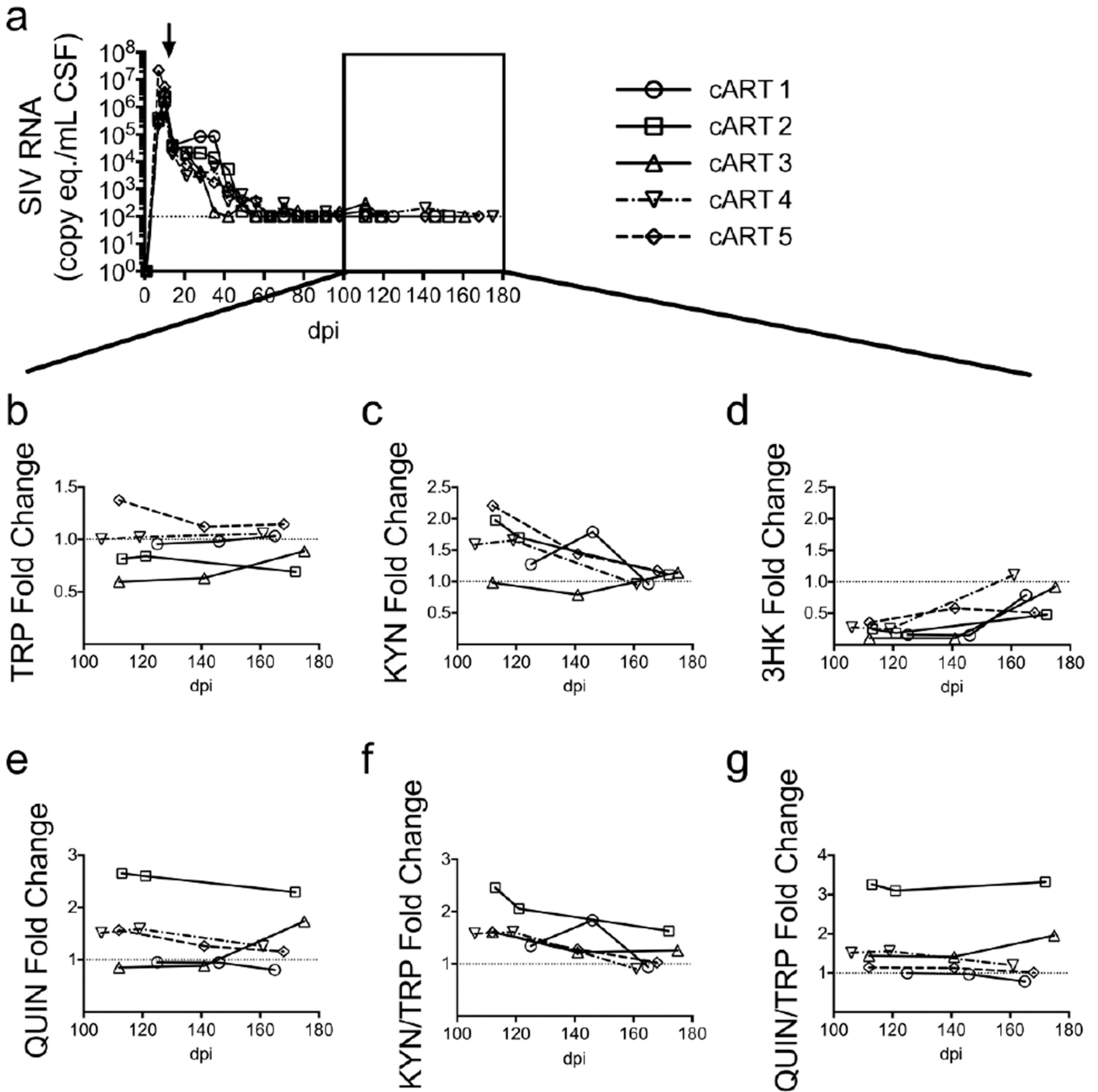
Fig. 6.

Low CSF QUIN/TRP ratios correspond with absence of neurological disease in well-suppressed, cART-treated animals. (**a**) Five SIV-infected macaques were treated with a 4-drug cART regimen beginning at day 12 p.i. (black arrow) that suppressed CSF viral loads to the limit of detection (100 copies/mL, represented by the dotted line) by 80 days p.i. The black box indicates time points during suppressive cART therapy at which metabolite levels were measured. (**b – f**) Three pre-infection CSF samples and three post-infection samples following suppression of CSF viremia to undetectable levels with cART were examined in

each animal for levels of TRP (**b**), KYN (**c**), 3HK (**d**), and QUIN (**e**), and for KYN/TRP (**f**) and QUIN/TRP ratios (**g**). Data in graphs **b** through **g** are presented as fold change over the average of the pre-infection values for each macaque, designated by the dotted line. The viral load data displayed in (**a**) has been modified from a previously published version (Zink et al. 2010).
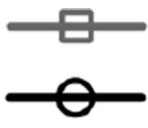
Fig. 7.
CSF KP metabolites correlate with brain levels during terminal infection. Spearman's rank correlations between matched terminal striatum and terminal CSF levels of TRP (**a**), KYN (**b**), 3HK (**c**), QUIN (**d**), KYN/TRP ratios (**e**), and QUIN/TRP ratios (**f**) are shown for 13 SIV-infected pigtailed macaques that did or did not receive cART. For all graphs, squares represent untreated animals with no or mild encephalitis (N = 3), circles represent untreated animals with moderate or severe encephalitis (N = 5), and triangles represent animals that were treated with cART and had no encephalitis at euthanasia (N = 5).
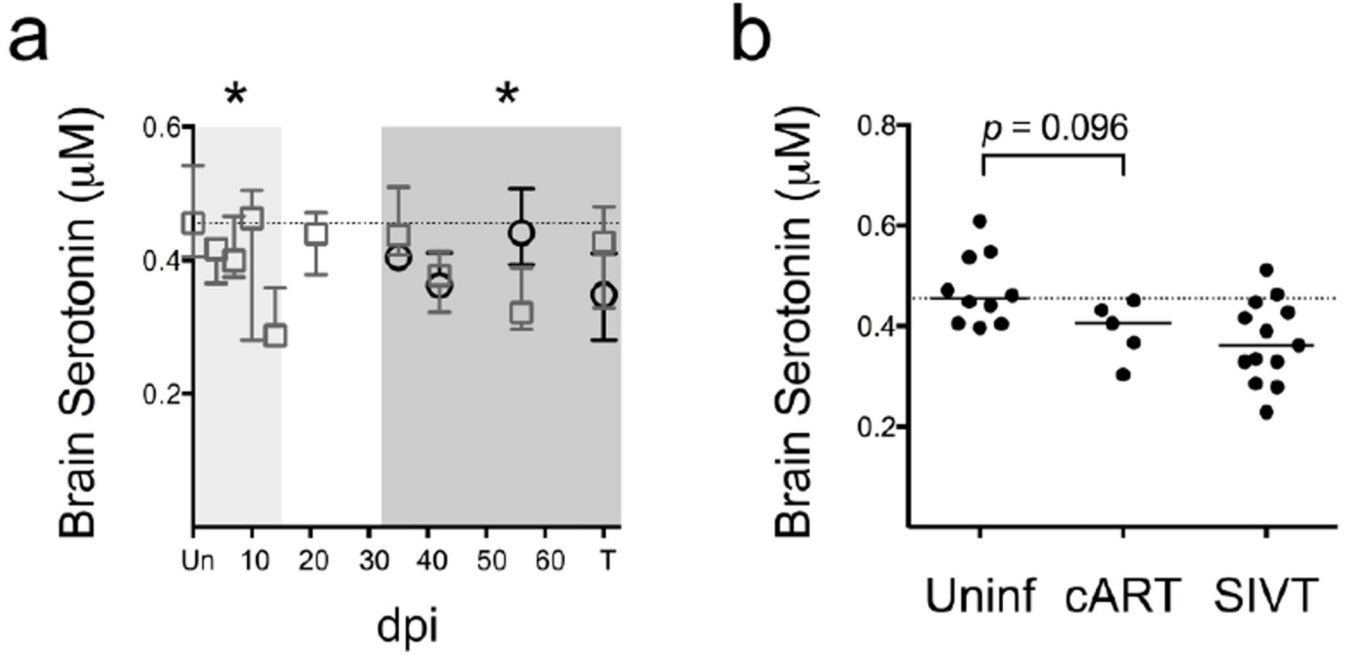
Fig. 8.

Serotonin is reduced in the brain during SIV infection and is partially restored by cART. (**a**) Serotonin levels in striatum from 79 animals euthanized at various points throughout infection are shown as medians with interquartile ranges. Asterisks (*) indicate whether the nadir during acute infection, or the total values during asymptomatic or chronic infection, were significantly different ($P < 0.05$) from uninfected controls by Mann-Whitney. Light grey shading represents the acute phase of infection (0–14 dpi), and dark grey shading represents the chronic phase of infection (≥35 dpi). (**b**) Striatal serotonin levels from uninfected animals (Uninf; N = 5), cART-treated, infected animals (cART; N = 5), and untreated, infected animals with terminal disease (SIVT; N = 13) are shown. The statistic shown is a Mann-Whitney U test comparison between Uninf and cART. In both graphs, the dotted line represents the median of uninfected controls.

Table 1

Summary of pigtailed macaque striatal samples euthanized at various days post infection and their corresponding neuropathology outcomes.

Days Post Infection	# None/Mild Encephalitis	# Moderate/Severe Encephalitis	Total
Uninfected	10	0	10
4	8	0	8
7	6	0	6
10	6	0	6
14	6	0	6
21	6	0	6
35	5	1	6
42	6	3	9
56	3	6	9
Terminal	5	8	13
cART	5	0	5